Identification of Plastics among Nonplastics in Mixed Waste by Remote Sensing Near-Infrared Imaging Spectroscopy. 2. Multivariate Image Rank Analysis for Rapid Classification

ARTICLE *in* ANALYTICAL CHEMISTRY · OCTOBER 1995

Impact Factor: 5.64 · DOI: 10.1021/ac00116a023

3 AUTHORS, INCLUDING:

Lutgarde Buydens
Radboud University Nijmegen
304 PUBLICATIONS **6,996** CITATIONS

SEE PROFILE

Anal. Chem. 1995, *67*, 3760–3766

Identification of Plastics among Nonplastics in Mixed Waste by Remote Sensing Near-Infrared Imaging Spectroscopy. 2. Multivariate Image Rank Analysis for Rapid Classification

D. Wienke,* W. van den Broek, and L. Buydens

Laboratory for Analytical Chemistry, Catholic University of Nijmegen, Toernooiveld 1, 6525 ED Nijmegen, The Netherlands

Macroscopic samples of household waste were experimentally characterized by a sequence of images, taken in four distinct wavelength regions by NIRIS. The obtained three-dimensional stack of images serves as individual fingerprint for each sample. A rapid data compression, followed by an abstract factor rotation of this stack into a spectroscopically meaningful intermediate four-element vector by a method called multivariate image rank analysis (MIRA), finally provided a single number. This number serves as decision limit for detection of plastics among nonplastic waste. The MIRA results are independent of sample size and sample position within the camera image. They are sensitive to only the type of sample material. MIRA was also found to be robust against image errors such as shadow or slight sample replacements between measurements.

Environmental and economic reasons make recycling of mixed industrial and household waste more attractive. The usually low value of waste can significantly be increased by sorting. Purer fractions of glass, metal, paper, and plastic waste can easier be reused, because they may be more easily reprocessed to higher valued products. Recently, spectroscopic and sensor methods in combination with rapid pattern recognition techniques were proposed for fine sortation of distinct types of postconsumer plastics.[1–3] Our laboratory has also developed an automated identification device for distinct types of plastics, based on a rapid remote near-IR diode array spectrometer combined with artificial neural networks as a real-time classifier.[4–6]

However, presorting of waste is a necessary step to get a stream of plastics for further fine sorting. Technologically, presorting is a more difficult step. Therefore, our laboratory is also developing an optical sensor device for presorting of mixed waste, and this will be described in the present work. This sensor device should be able to identify the plastics within the stream of mixed waste. This research is part of European project SIRIUS (Sensors and Artificial Intelligence for Recognition and Identification of Used Plastics), in cooperation with the Institute for Chemical and Biochemical Sensor Research (ICB) in Münster, Germany.

Based on a feasibility study on infrared spectra of several materials in household waste, the idea has been developed by the authors to use near-infrared imaging spectroscopy (NIRIS) for discrimination between plastics and nonplastics in waste. This idea is based on distinct spectroscopic fingerprints of plastics and nonplastics in the optical near-IR region (Figure 1a,b). Near-IR spectra of plastics (Figure 1a) show two significant peaks: one in the central near-IR region (first overtone around 1600 nm) and one at the upper end of the wavelength scale (combination bands, around 2300 nm). Nonplastics from household garbage such as glass, ceramics, and metals provide decreasing spectral patterns with increasing near-IR wavelength. Only natural polymers such as paper and wood give a spectral peak structure that is more similar to that of particular plastics than to metal, glass, and ceramics (Figure 1b).

One could ask, why not use a rapid scan near-IR spectrometer for this classification task? What would be the added value of NIRIS compared to a classical near-IR spectrometer? The answer lies less in the analytical–spectroscopic field and more in the process–analytical field. NIRIS provides more than the type of sample material. An near-IR image additionally gives an estimate of sample shape and sample size. In recycling technology, sample shape and sample size are additional important descriptors for identification and sorting. One may be interested, for example, in forming separate fractions of bottles and cans from the same material. NIRIS has a second technological advantage compared with classical "single spot" near-IR spectroscopy. Varying size and position from sample to sample at the moving conveyor belt cause focus problems for a remote spectrometer with a single focused measuring spot. In contrast to that, a spectroscopic camera with a wide angle of view can solve the focus problem better than a single spectrometer beam. It provides a particular redundance in analytical information, giving somewhat more freedom to on-line process analysis. The redundancy in NIRIS data can be removed again afterward with chemometrical tools, as will be demonstrated in the present study. However, the alternative idea, to use a rapid scan near-IR spectrometer for presorting of waste instead of a spectroscopic imaging camera, is under consideration within the SIRIUS project, too. The results

(1) Eisenreich, N.; Knull, H.; Theines, E. Presented at the 23rd Annual Waste Management Conference of Energetic Materials and Polymers, Inst. Chem. Tech Karlsruhe, Germany, 1992; 59/1–59/12.
(2) Ritzmann, H. P.; Schudel, D. *Kunststoffe* **1994**, *84*, 582–584.
(3) Alam, M. K.; Stanton, S. L. *Process Control Quality* **1993**, *4*, 245–252.
(4) Wienke, D.; van den Broek, W.; Melssen, W.; Buydens, L.; Feldhoff, R.; Kantimm, T.; Huth-Fehre, T.; Quick, L.; Winter, F.; Cammann, K. *Anal. Chim. Acta*, in press.
(5) Huth-Fehre, T.; Feldhoff, R.; Kantimm, Th.; Quick, L.; Winter, F.; Cammann, K.; van den Broek, W.; Wienke, D.; Melssen, W.; Buydens, L. *J. Mol. Struct.* **1995**, *348*, 143–146.
(6) Wienke, D.; van den Broek, W.; Schoenmakers, J.-W.; Buydens, L.; Huth-Fehre, T.; Feldhoff, R.; Kantimm, T.; Cammann, K. *Chemom. Intell. Lab. Syst*, in press.

0003-2700/95/0367-3760$9.00/0

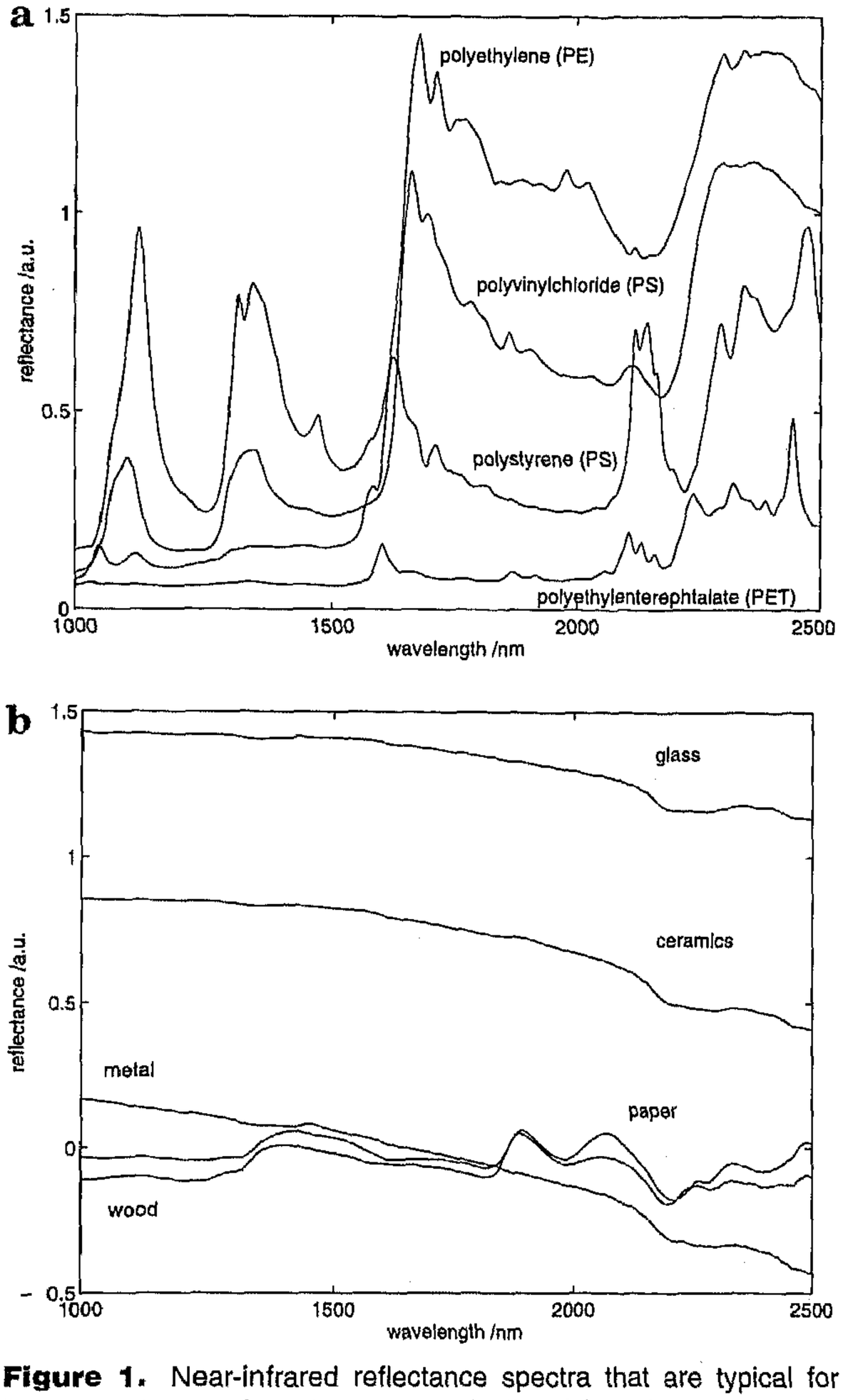

Figure 1. Near-infrared reflectance spectra that are typical for important types of postconsumer plastics (a) and postconsumer nonplastics (b). Spectra were taken by a NIRSystems 6500 spectrometer using a DRIFT unit for transflectance measurements.

will reported later. The present work will focus on the use of a remote operating wide optical range high-speed digital (near-)IR camera as a multivariate optical sensor.

Such fast digital (near-)IR imaging devices, based on advanced semiconductor materials (InSb, InGaAs, HgCdTe), became available in the last few years for civil research as rather typical products from military and space technology. They substitute the near-IR videcons used, for example, by Robert et al.[7], McClure,[8,9] and Geladi et al.[12] in their pioneering studies of NIRIS. Recently, Lewis, Levin, and Treado[13,14] reported first results with their InSb focal plane diode array for spectroscopic near-IR microscopy.

(7) Robert, P.; Bertrand, D.; Devaux, M. F. *NIR News* **1991**, *2* (2), 9–10.
(8) McClure, W. F. *NIR News* **1991**, *2* (2), 8.
(9) McClure, W. F. *Anal. Chem.* **1994**, *66*, 43A–53A.
(10) Geladi, P.; Isaksson, H.; Lindquist, L.; Wold, S.; Esbensen, K. *Chemom.* Intell. Lab. Syst. **1989**, *5*, 209–220.
(11) Geladi, P.; Esbensen, K. In *SAR and Environmental Studies*; Devillers, J., Karcher, W., Eds.; Kluwer Scientific Publishers: Amsterdam, 1991; pp 415–445.
(12) Geladi, P.; Grahn, H.; Lindgren, F. In *Applied Multivariate Analysis in SAR and Environmental Studies*; Devillers, J., Karcher, W., Eds.; Kluwer Scientific Publishers: Amsterdam, 1991; pp 447–478.
(13) Lewis, E. N.; Levin, I. A. *Appl. Spectrosc.* **1995**, *49* (5) 673–678.
(14) Treado, P. J.; Levin, I. W.; Levis, E. N. *Appl. Spectrosc.* **1994**, *48* (5), 607–615.

In the present macroscopic application, the (near-)IR cameras need to be fast enough for use on a running conveyor belt with a typical transportation speed for waste of 2 m/s. Another requirement is that the data processing has to be done in real-time. This can be reached by optical data processing or by fast computers and efficient chemometrical algorithms.

The present work will describe such an experimental presorter developed in our laboratory. Furthermore, the MIRA algorithm will be introduced as one chemometrical possibility to extract the correct material type (plastics versus nonplastics) from a three-dimensional stack of near-IR images.

THEORY

Assumptions. NIRIS measurements of chemical samples by a camera in the optical near-IR range can be compared with an absorption measurement (or a reflectance measurement) in optical spectroscopy. Namely, to get the single desired netto image of a sample, $\mathbf{I}_{n,m}$, forming a data matrix of intensity values, measured with $n \times m$ pixels, one needs in total three measurements: first, the brutto image, $\mathbf{I}_{n,m}^{\text{ref+sample}}$, showing the sample placed in a sample background (single piece of waste material at the conveyor belt); second, the pure image of the neutral background, $\mathbf{I}_{n,m}^{\text{ref}}$, that simultaneously will serve as an independent reference image (usually the empty conveyor belt). (As in spectroscopy, a reference image corrects for the spectrum of the camera optics, for the spectrum of the illumination source and for characteristical sensitivity function of the detector array.); third, the dark current level image of the camera itself, $\mathbf{I}_{n,m}^{\text{dark}}$, to correct for a noise offset of the detector array. As in absorption theory for optical spectroscopy, the netto image is obtained, then, by combining all three measured images:

$$\mathbf{I}_{n,m} = 1 - (\mathbf{I}_{n,m}^{\text{ref+sample}} - \mathbf{I}_{n,m}^{\text{dark}}) / (\mathbf{I}_{n,m}^{\text{ref}} - \mathbf{I}_{n,m}^{\text{dark}}) \qquad (1)$$

An example helps to explain this expression. Assume a camera with a focal plane array of 64 × 64 pixels, each having 10-bits pixel resolution (see also Experimental Section). Each pixel can thus provide digital measurements (integers) between 0 and 1023 (respectively 1 and 1024). If one closes the shutter of the camera lens, one gets the dark image of the detector. For a near-IR camera with a semiconductor array (InSb, InGaAs, HgCdTe, etc.), it usually has a noise level between 100 and 400 gray values. Assume, for example, a noise level of 256 gray values: the maximum range of 1024 possible intensity values shrinks to the real range of 1024 − 256 = 768. This is, in fact, only a dynamical detector range of 9.5-bit instead of the announced 10-bit. Additionally, one has to divide by a reference image, $\mathbf{I}_{n,m}^{\text{ref}}$, that plays the role of the 100% reference intensity in optical spectroscopy, sent through an empty spectrometer (without sample). Finally, a zero background level is obtained for the netto image $\mathbf{I}_{n,m}$ in eq 1 by substracting the whole right expression from 1.

If the same sample will be imaged at p distinct wavelength at identical position and with identical background, one will get a so-called stack of images. A capitalized, underlined, boldface letter, $\underline{\mathbf{X}}_{n,m,p}$, is used for such a three-dimensional data array. Two directions of this data stack originate from image geometry $n \times m$ and the third direction from the p distinct wavelengths.

Such multiwavelength images have been taken for many years by civil and military space satellites from the earth's surface and evaluated by rather classical image processing techniques and

by multivariate methods such as principal component analysis (PCA). The same idea of multiwavelength imaging (or "imaging spectroscopy") and PCA, extended by other multivariate methods such as PLS regression, was proposed for numerous chemical applications by Geladi et al.,[10-12] Esbensen and Geladi,[15] and Grahn et al.[16] Under the mathematical assumption that such a stack of images is a linear combination of individual images from several chemical or physical "hidden components", these authors demonstrated that PCA is an excellent tool to find the hidden component images by decomposing this three-dimensional stack. The elegance of this is that the principal components (scores) can be presented as images again after a suitable backtransformation, which helps in gaining a visual understanding of the nature of the hidden components. The present MIRA approach basically uses a comparable idea under very different experimental assumptions. First, in contrast to the former, only one chemical sample is expected in the image. (Technically, this can be guaranteed in each modern mechanical waste sortation plant.) Second, according to eq 1, the pixels belonging to the pure background (nonobject pixels) have values close to zero. Third, artifacts such as shadow, specular reflectance, and interferences cannot be completely avoided. In the preceding work,[17] it has been proven that most of these effects can be linearely separated from the sample part by singular value decomposition. Fourth, the single waste sample will move slightly in time during the p measurements, caused by the conveyor belt movement.

Multivariate Image Rank Analysis (MIRA). A three-dimensional stack of images from a single waste sample forms a three-dimensional data array $\underline{\mathbf{X}}_{n,m,p}$ with $i = i-n$ image pixels in one image direction and $j = 1-m$ image pixels in the other image direction, and with $k = 1-p$ wavelength slides in the third direction. $\underline{\mathbf{X}}_{n,m,p}$ is unfolded to a two-dimensional data array (matrix), $\mathbf{Z}_{nm,p}$, with p columns and $n \times m$ rows. In practice, unfolding costs no extra computation time, because a digital camera is read out pixel by pixel, which means that the images always already unfolded reach the computer memory. Each of the p image slices thus forms a single column vector inside $\mathbf{Z}_{nm,p}$, and all former rows of the original image form behind each other a long, one-dimensional data string. In this way, the geometrical information about the object shape and its position is lost because the unfolding operation destroyed the pixel neighborhood interrelationships. However, at this moment, we were interested only in the material type. The required spectroscopic information is still present in $\mathbf{Z}_{nm,p}$. The p columns of $\mathbf{Z}_{nm,p}$ form a small spectrum for each image pixel (row). One possible means of material analysis would be a row-by-row scan of $\mathbf{Z}_{nm,p}$, combined with a check of each of the $n \times m$ spectra. Simple statistics for all $n \times m$ rows would provide the number of background spectra, the number of sample spectra, and the spectra. However, such simple counting works only for simulated images where noise, shadow, and mirror effects are absent. In the MIRA approach, we assume that $\mathbf{Z}_{nm,p}$ contains the desired information but in a hidden way among these several undesired influences.

Multiplying pixel i by itself can be considered as multiplication of the transpose $\mathbf{z}_i^T$ of its spectral patterns with this pattern $\mathbf{z}_i$ to a matrix $\mathbf{C}_{p,p}^{\text{sample,i,i}}$ of dimension $p \times p$. This matrix can be written by the square of a new vector $\mathbf{s}$ of standard length 1 and a scaling constant a with

$$\mathbf{z}_i^T\mathbf{z}_i = \mathbf{C}_{p,p}^{\text{sample,i,i}} = (\mathbf{z}_i^T/||\mathbf{z}_i||)||\mathbf{z}_i||^2(\mathbf{z}_i/||\mathbf{z}_i||) = \mathbf{s}_i^T a \mathbf{s}_i \quad (2)$$

This constant a is thus the squared length of $\mathbf{z}_i$. Because $\mathbf{z}_i$ is the spectrum of the sample pixel, then $\mathbf{s}_i$ is a standardized spectrum of length 1 of the pixel. A pairwise multiplication over all pixels belonging to the sample within the entire image,

$$\mathbf{C}_{p,p}^{\text{sample}} = \sum_{i=1}^{\text{sample pixels}} (\mathbf{z}_i^{\text{sample,T}}\mathbf{z}_i^{\text{sample}}) = \sum_{i=1}^{\text{sample pixels}} (\mathbf{s}_i^{\text{sample,T}} a^{\text{sample}} \mathbf{s}_i^{\text{sample}}) \quad (3)$$

still provides a matrix $\mathbf{C}_{p,p}^{\text{sample}}$ of dimension $p \times p$, which is now the total sum of all the pairwise vector products. Another matrix of dimensions $p \times p$ can be found for all pixels of the image background, $\mathbf{C}_{p,p}^{\text{bg}}$, with

$$\mathbf{C}_{p,p}^{\text{bg}} = \sum_{i=1}^{\text{bg pixels}} (\mathbf{z}_i^{\text{bg,T}}\mathbf{z}_i^{\text{bg}}) = \sum_{i=1}^{\text{bg pixels}} (\mathbf{s}_i^{\text{bg,T}} a^{\text{bg}} \mathbf{s}_i^{\text{bg}}) \quad (4)$$

A similar expression can be given for pixels from a shadow, $\mathbf{C}_{p,p}^{\text{shadow}}$:

$$\mathbf{C}_{p,p}^{\text{shadow}} = \sum_{i=1}^{\text{shadow pixels}} (\mathbf{z}_i^{\text{shadow,T}}\mathbf{z}_i^{\text{shadow}}) = \sum_{i=1}^{\text{shadow pixels}} (\mathbf{s}_i^{\text{shadow,T}} a^{\text{shadow}} \mathbf{s}_i^{\text{shadow}}) \quad (5)$$

and for pixels that changed from sample pixels to background pixels because of the conveyor belt movement, $\mathbf{C}_{p,p}^{\text{move}}$, measurement noise, $\mathbf{C}_{p,p}^{\text{noise}}$, and other artifacts and undesired image effects. Thus, the unfolded stack of images, multiplied by its left transpose, can thus be rewritten as a sum:

$$(\mathbf{Z}^T\mathbf{Z})_{p,p} = \mathbf{C}_{p,p}^{\text{sample}} + \mathbf{C}_{p,p}^{\text{bg}} + \mathbf{C}_{p,p}^{\text{shadow}} + \mathbf{C}_{p,p}^{\text{move}} + \cdots + \mathbf{C}_{p,p}^{\text{noise}} \quad (6)$$

As already mentioned, this linear separability of several undesired image artifacts, such as distinct types of shadow, background, or specular reflection, has already been experimentally demonstrated.[17] It forms an important basis for the applicability of the entire MIRA approach.

According to eqs 2–5, these individual matrices in eq 6 can be further decomposed into their standardized spectral profiles $\mathbf{s}$ and the scaling factor a, giving the following expression:

$$(\mathbf{Z}^T\mathbf{Z})_{p,p} = \mathbf{s}^{\text{sample,T}} a^{\text{sample}} \mathbf{s}^{\text{sample}} + \mathbf{s}^{\text{bg,T}} a^{\text{bg}} \mathbf{s}^{\text{bg}} + \mathbf{s}^{\text{shadow,T}} a^{\text{shadow}} \mathbf{s}^{\text{shadow}} + \cdots + \mathbf{s}^{\text{noise,T}} a^{\text{noise}} \mathbf{s}^{\text{noise}} \quad (7)$$

On the other hand, a classical singular value decomposition

(15) Esbensen, K.; Geladi, P. *Chemom. Intell. Lab. Syst.* **1989**, *7*, 67–86.
(16) Grahn, H.; Szevenyi, N. M.; Roggenbuck, M. W. *Chemom. Intell. Lab. Syst.* **1989**, *7*, 87–93.
(17) van den Broek, W.; Wienke, D.; Melssen, W.; de Crom, K.; Buydens, L. Anal. Chem. **1995**, *67*, 3753–3759.

(SVD) of $(\mathbf{Z}^T\mathbf{Z})_{p,p}$ would be written as

$$(\mathbf{Z}^T\mathbf{Z})_{p,p} = \mathbf{u}^{source1}\lambda^{source1}\mathbf{e}^{source1,T} + \mathbf{u}^{source2}\lambda^{source2}\mathbf{e}^{source2,T} + \mathbf{u}^{source3}\lambda^{source3}\mathbf{e}^{source3,T} + \cdots + \mathbf{u}^{source4}\lambda^{source4}\mathbf{e}^{source4,T} \quad (8)$$

with matrix $\mathbf{U}$ = singular vectors $(\mathbf{Z}^T\mathbf{Z})^T_{p,p}(\mathbf{Z}^T\mathbf{Z})_{p,p}$, matrix $\mathbf{E}$ = singular vectors $(\mathbf{Z}^T\mathbf{Z})_{p,p}(\mathbf{Z}^T\mathbf{Z})^T_{p,p}$ and λ the diagonal matrix of singular values.

Equation 8 is a decomposition of the image stack into abstract sources of variation. A chemically meaningful rotation of this abstract solution is required. However, eqs 7 and 8 show a high similarity and offer a way to estimate the desired standardized spectral profiles $\mathbf{s}$ by a SVD under well-defined experimental assumptions (see below). Geladi et al.[10] discussed this way as a rapid numerical possibility to estimate the desired scores images $\mathbf{T}$ from a PCA decomposition of $\mathbf{Z}$:

$$\mathbf{Z} = \mathbf{TL} \quad (9)$$

via their PCA loadings $\mathbf{L}$ and PCA eigenvalues $\mathbf{D}$ obtained by

$$(\mathbf{Z}^T\mathbf{Z}) = \mathbf{L}^T\mathbf{DL} \quad (10)$$

However, we were less interested in the scores image $\mathbf{t}$ but more in a quantitative prediction of the waste sample's individual spectral profile $\mathbf{e}^{sample}$ (identical with $\mathbf{u}^{T,sample}$) from the image stack to extract the correct material type.

The point of the MIRA approach to maximize the contribution of the matrix $\mathbf{C}^{sample}_{p,p}$ in expression 6 while minimizing the contribution of the remaining terms by experiment. In other words, the MIRA approach tries to force $(\mathbf{Z}^T\mathbf{Z})_{p,p}$ into a matrix of rank $r = 1$. Expression 1, for example, helps to force the background term $\mathbf{C}^{bg}_{p,p}$ toward a zero matrix. The shadow term in eq 6 becomes small with an intelligent sample illumination. The term $\mathbf{C}^{move}_{p,p}$ can be minimized if the measurement speed is some magnitude higher than the movement of the conveyor belt with the sample. If the object of interest has a significant absorption within the total image, it will always dominate the first-rank component. One can consider the SVD step also as a rotation of the matrix $(\mathbf{Z}^T_{nxm,p}\mathbf{Z}_{nxm,p})_{p,p}$ into a new coordinate system $\mathbf{U}_{p,f}$, whereby the rotation matrix is equal to

$$\mathbf{R}_{f,p} = \mathbf{V}_{f,f}\mathbf{E}^T_{f,p} \quad (11)$$

providing the new axis that corresponds to the order f of rank components. As mentioned above, the dominating rank of the sample in the image will force this rotation in a spectroscopically desired direction. The ideal case would be for the column vector $\mathbf{u}_1$ to approximate $\mathbf{s}^{sample}$ as close as possible. Clearly, the more dominant the rank-one component, the better this approximation will be.

The last step of the MIRA model is the extraction of a decision limit from the predicted spectra $\mathbf{u}$ profile of the sample. For this we make use of the normality property of $\mathbf{u}_1$ (length = 1!) and of an additional spectroscopic trick. The p filters are placed in such a way in the spectrum that for each filter that is placed at a characteristic absorption peak (Figure 1a), a second one is placed in a valley (absorption minimum) close to the peak. In the case of plastics identification, we used two peaks in the near-IR

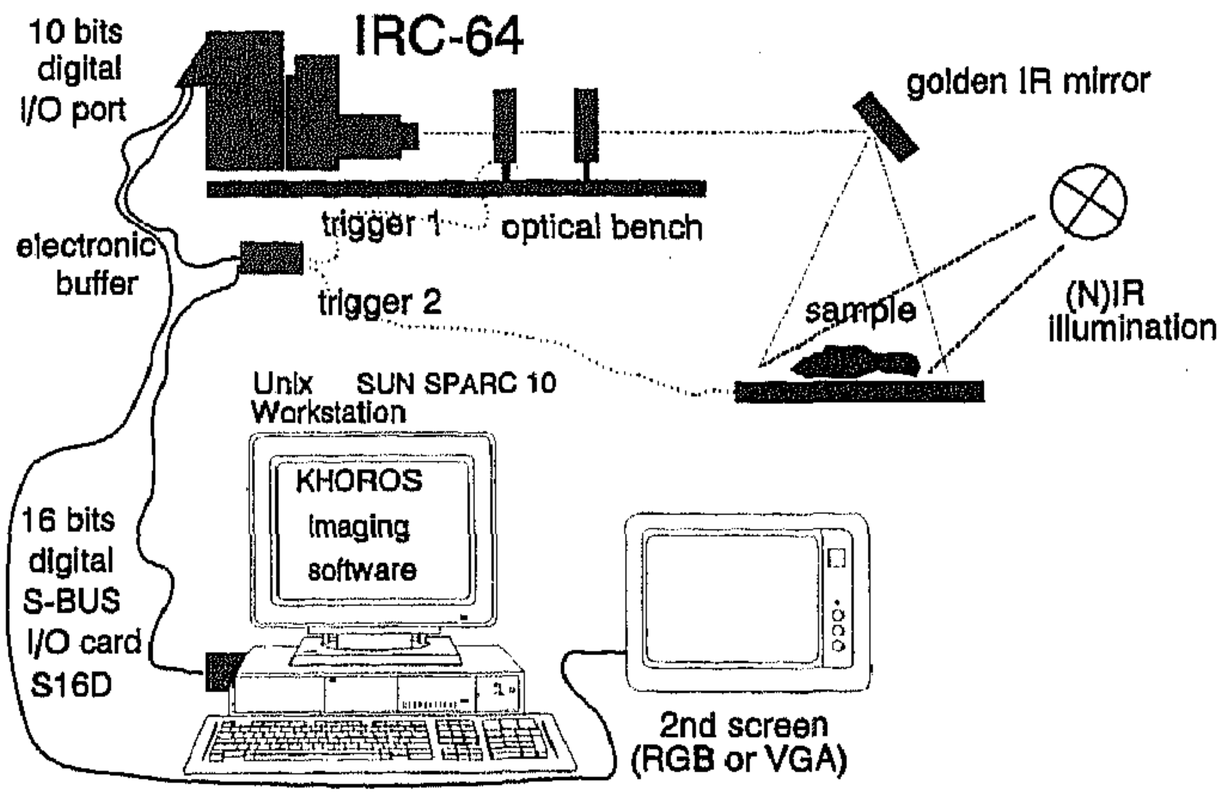

Figure 2. Experimentally realized laboratory setup for presorting of mixed postconsumer waste. Near-infrared images from the same sample, placed and illuminated on a conveyor belt, can be taken in p wavelength regions. The wavelength regions are selected by a rotating wheel with interference filters, placed in front of the camera. The obtained image stack is on-line processed by a dedicated Unix workstation, running in stand-alone mode.

spectrum where plastics show a high absorbance compared to nonplastics. According to Figure 1a, the high-intensity filters can be placed, for example, around 1700 and 2400 nm (see Experimental Section). Based on this trick and on the normality property of $\mathbf{u}_1$, the calculated decision value for an arbitrary sample,

$$B^{sample} = \left(\sum_{k=1}^{p/2} u^2_{k,peaks} \Big/ \sum_{k=1}^{p/2} u^2_{k,valleys}\right) \quad (12)$$

summarizes all elements in the predicted $\mathbf{u}$ vector corresponding to peak wavelengths, divided by the sum over all elements in $\mathbf{u}$ corresponding to non-peak wavelength. The value for B will thus for spectra like that in Figure 1a be much larger than 1 (plastics). For spectra like that in Figure 1b, the predicted value for B will be significantly smaller than 1 (metal, stone, ceramics) or close to 1 for wood and paper (a little bit larger or smaller than 1). In this way, the former original three-way data array, $\underline{\mathbf{X}}_{n,m,p}$, from the camera measurement of one waste sample is compressed to a single number B as a scalar decision limit for future control of an automated waste sorter.

EXPERIMENTAL SECTION

A digital infrared diode array camera IRC-64 (Cincinatti Electronics Inc., Mason, OH) has been mounted at an optical bench on the laboratory wall (Figure 2). The camera has a 64 × 64 pixels focal plane diode array of nitrogen-cooled InSb that is sensitive in the wavelength region from 1.1 to 5.0 μm. A cold shield inside the camera blocks undesired infrared background radiation above 4.6 μm but allows radiation to pass between 1.0 and 4.6 μm. An IR optics (CaF_2, transparent at 2.3−4.5 μm) and a near-IR optics (BK7 glass, transparent at 0.3−2.75 μm) allow us to obtain mid- and near-IR measurements. Via an electronic buffer, concerning a trigger input/output, the camera has been connected to a high-speed 16-bit digital interface S16D (S-Bus card made by EDT Inc., Beaverton, OR). The stream of digital image data is written by the S16D I/O card directly into the 32 MB RAM of a SUN Sparc 10 (Unix workstation) in real-time. This enables us, via the digital I/O port (10 and 12 bits, respectively), the technical

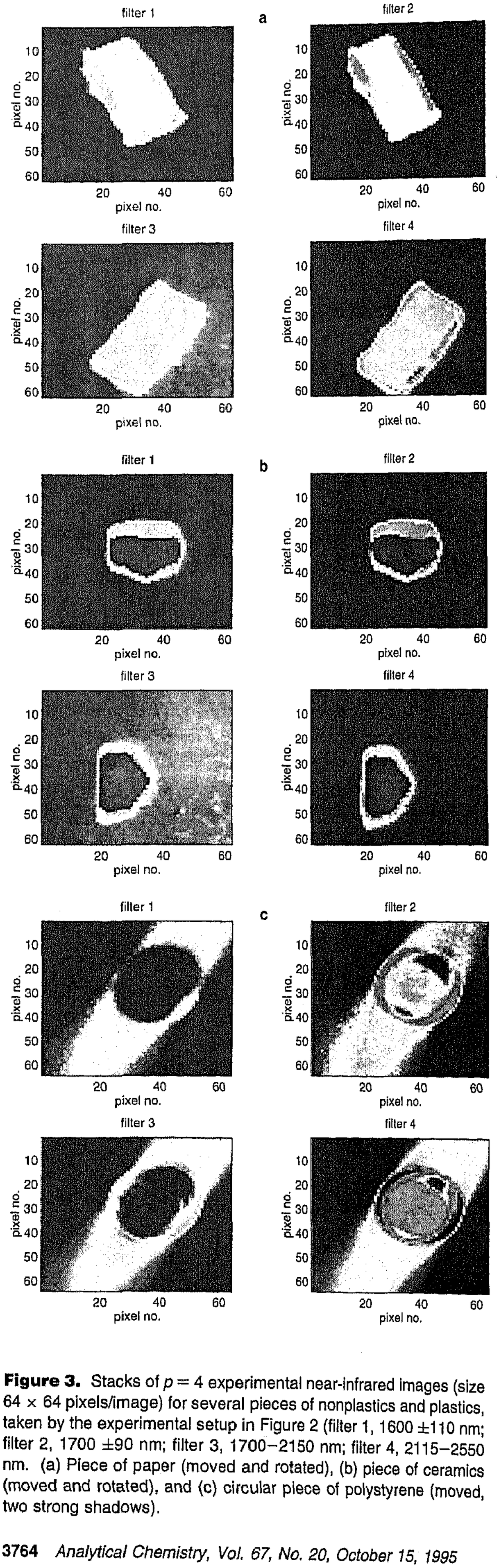

Figure 3. Stacks of $p = 4$ experimental near-infrared images (size 64 × 64 pixels/image) for several pieces of nonplastics and plastics, taken by the experimental setup in Figure 2 (filter 1, 1600 ±110 nm; filter 2, 1700 ±90 nm; filter 3, 1700−2150 nm; filter 4, 2115−2550 nm. (a) Piece of paper (moved and rotated), (b) piece of ceramics (moved and rotated), and (c) circular piece of polystyrene (moved, two strong shadows).

possibility of high-speed measurements with up to 52 images/s. Simultaneously, the less well resolved 8-bit analog infrared image can be visualized on a second screen in real-time by using the alternative RGB or the VGA output port of the IRC. Reading the digital data directly from the camera avoids any further analog–digital conversion (or vice versa). An additional advantage is that no framegrabber is needed. In this way, the digital images are not disturbed by any noise caused by data conversion processes. Simultaneously, the maximum camera speed of 52 digital images/s of size 64 × 64 pixels is used. The real-time measurement is done under the large KHOROS imaging software package (University of New Mexico, Albuquerque, NM). The IRC-64 can be directly on-line called under KHOROS by a computer mouse-supported operation. A symbolic camera icon appears within the graphical CANTATA user interface of KHOROS on the workstation screen. In this way, the camera becomes operational. The data stream from the camera can be linked on-line via the workstation's 32 MB RAM to all software devices available in KHOROS, such as mathematical filters, image transformations, image analysis algorithms, and multivariate data analysis. Communication software between the S16D card and KHOROS and the electronic installation has been realized by Starling Consultancy (Hengelo, The Netherlands). Complete infrared movies can be measured by the IRC-64 and then presented by KHOROS by real-time visualization of the movie out of the workstation's RAM. IRC-64 images can be saved to disk in several formats by KHOROS. In this way the images can be read into other imaging software, such as MATLAB, and into self-written programs under the Unix operating system. A rotable filter wheel at the optical bench with up to $p = 8$ filters helps to measure the same sample in distinct desired wavelength regions. For the present experiments, we used four near-IR interference filters from Spectrogon (Sweden) with the following parameters (compare with spectra in Figure 1): narrow band pass filter 1 (1600 ± 110 nm), narrow band pass filter 2 (1700 ± 90 nm), broad band filter 3 (1700−2150 nm), and broad band filter 4 (2115−2550 nm).

Further equipment, such as a pin-hole setup, mirrors, and (near-)IR-illumination sources, were mounted. The pixelwise recalibration of the camera is done by a so-called uniformity module using a cool and a hot emission sources. A sanded plate, made from aluminum, provides a neutral, scattering, metallic background for (near-)IR radiation and for measurement of the reference image, $\mathbf{I}^{ref}_{64,64}$.

SOFTWARE AND COMPUTATIONS

Four images per sample were saved by KHOROS to hard disk and then read into MATLAB (Unix). The MIRA algorithm, as described in the Theory section, has been completely developed and implemented in MATLAB by the author. In the mean time, MIRA has been also implemented and tested in C language. This now allows use of MIRA outside KHOROS by direct access in real-time and in on-line mode to the IRC-64 camera to run the complete presorter setup automatically.

RESULTS AND DISCUSSION

Different but typical waste materials were analyzed by the described experimental setup. Macroscopic pieces of several centimeters in size made from paper, wood, glass, metal, ceramics, and stone served as typical nonplastics. Pieces of white polystyrene, yellow polyethylene, and dark blue polypropene were

Table 1. Experimental Image Stacks of Size 64 × 64 × 4 for Distinct Plastics and Nonplastic Samples (Partly Given in Figure 3), Decomposed by the MIRA Approach via Eqs 1–8[a]

true material type	sample moved during measurement?	predicted dicision border B	corresponding eigenvalue λ_1	λ_2	λ_3	λ_4
white polystyrene	no	3.73	374.6	109.3	9.7	2.43
white polystyrene	yes	1.41	670.1	70.1	23.3	16.1
dark blue polypropene	no	1.96	615.9	23.8	4.6	3.0
dark blue polypropene	yes	1.59	659.3	34.5	12.1	4.6
stone	yes	0.88	688.2	200.9	10.9	1.5
ceramics	no	0.90	339.5	7.3	3.9	1.5
paper	no	0.25	256.7	29.9	14.1	2.3
paper	yes	1.13	331.3	138.2	19.04	6.6
yellow polyethylene	no	2.22	696.1	22.89	9.7	3.91
yellow polyethylene	yes	1.96	598.7	138.2	41.0	13.6
aluminum	no	1.10	640.8	207.6	166.8	71.0
aluminum	yes	0.82	597.8	212.7	96.6	63.1
copper	no	0.87	316.9	33.3	9.5	5.3
copper	yes	0.90	302.6	28.7	14.0	3.0
brown glass	no	0.82	570.1	55.7	15.6	12.4
brown glass	yes	0.80	535.5	60.0	19.8	8.7
white glass	no	1.07	53.8	26.9	5.9	2.9
white glass	yes	0.00	517.8	38.7	17.9	13.7
wood	no	1.53	156.7	19.3	9.2	1.9
wood	yes	0.02	401.2	130.9	20.7	2.0

[a] If the calculated decision value B for the images is large, a plastic is found. See Table 2 for the corresponding standardized spectral patterns, $\mathbf{u}_1$, for selected samples.

Table 2. Predicted Spectral Elements of $\mathbf{u}_1$ Profiles for the samples, Given in Table 1, Extracted by the MIRA Approach from the Image Stacks[a]

true material type	sample moved during measurement?	**u** profile $\mathbf{u}_1$	$\mathbf{u}_2$	$\mathbf{u}_3$	$\mathbf{u}_4$
white polystyrene	no	0.15	0.55	0.30	0.76
white polystyrene	yes	0.37	0.49	0.38	0.70
dark blue polypropene	no	0.26	0.50	0.52	0.65
dark blue polypropene	yes	0.35	0.48	0.51	0.62
stone	yes	0.50	0.49	0.52	0.47
ceramics	no	0.52	0.51	0.50	0.46
paper	no	0.88	0.41	0.12	0.18
paper	yes	0.30	0.06	0.62	0.73
yellow polyethylene	no	0.15	0.42	0.54	0.71
yellow polyethylene	yes	0.16	0.39	0.56	0.71
aluminum	no	0.53	0.58	0.44	0.44
aluminum	yes	0.54	0.48	0.51	0.47
copper	no	0.52	0.46	0.51	0.51
copper	yes	0.53	0.49	0.49	0.48
brown glass	no	0.53	0.50	0.52	0.44
brown glass	yes	0.55	0.49	0.51	0.46
white glass	no	0.40	0.52	0.57	0.50
white glass	yes	0.98	−0.02	0.19	−0.02
wood	no	0.34	0.27	0.53	0.73
wood	yes	0.98	0.13	−0.15	−0.06

[a] Compare the $\mathbf{u}_1$ profiles with corresponding near-IR spectra in Figure 1.

characterized as easy and as a difficult plastic samples (dark colored samples give near-IR spectra with a bad S/N ratio). Looking to selected near-IR images (Figure 3), one can already see the difference in absorption ratios between the different wavelength regions for different materials. The piece of paper (Figure 3a) shows an absorption pattern that lies between those of ceramics (Figure 3b, nearly no differences) and the piece of plastic (Figure 3c, remarkable absorption contrasts). Realistic situations at a moving conveyor belt in a waste sortation plant (sample shadow, sample replacement, mirror reflection) were simulated by irregular sample illumination and sample movement during measurement (rotation, translation).

The summarized results for all experimental images and additional samples (Tables 1 and 2) show that the MIRA approach works for almost all samples, as theoretically predicted. For all plastics, the predicted B value is, as desired, significant larger than 1 and often close to or larger than 2. The reverse trend (smaller than or around 1) was found for all nonplastics. However, in some cases, the B value for some nonplastics deviates a little from the expectations. An example is the piece of polished aluminum ($B = 1.10$). One reason could be that the background was a sanded aluminum plate giving only minimal contrast. A second example is the piece of paper. After a strong rotation by 90° and a moderate movement, the former correct B value for paper of 0.25 raised over the decision border to a value of 1.13. This is still lower as for all plastics but gives the general impression that small changes in position are tolerated by the MIRA approach. But if the overlap between sample pixels is lost within the same image stack by too much sample movement, then the correlation between them is lost and a second significant singular value is generated, providing a wrong **u**-profile. One can see this, for example, for paper in Table 1; the second eigenvalue is raised if a sample is moved between two filter measurements. A third negative example is the piece of wood ($B = 1.53$).

However, the first eigenvalue dominates in all cases the other three for all measured sample image stacks (Table 1). This one condition is necessary to get a suitable estimate **u** of the searched spectral profile **s** of each sample in order to obtain in this way a correct prediction of the material class via the B criterion.

Another interesting result has been found. Shadows, mirror reflections, and other types of irregular illumination obviously do not play as negative a role as expected. In other words, these effects seem to be nearly independent of wavelength, so they form together with the background a linear independent hidden component with minor influence. The constancy of their absorption intensity decouples these effects in the components space from the variation of the sample absorption with wavelength. For recycling practice, that means that the conveyor belt does not need to be illuminated by an extreme homogeneous light source, but only by a simple near-IR lamp.

The estimates **u** for the desired standardized spectral profiles **s** (Table 2) show a good correlation with the true near-IR spectra, as given in Figure 1a for plastics and in Figure 1b for nonplastics. The **u** profiles for plastics correctly reflect the theoretically expected spectral pattern low–high–low–high determined from the placement of the four filters. The decreasing intensity trend with increasing wavelength of the **u** profiles for stone and ceramics agrees almost perfectly with the spectra of ceramics (or glass) (Figure 1b). For paper and metal, the general trend is also correct, but differences in some details are stronger than for the other materials. Most of the problems are caused by the optical system (transmission spectrum of the camera lens, emission spectrum of the near-IR illumination source). At this moment, a boron crown glass lens (BK7) is used that shows between 2100 and 2700 nm a significant decrease in transmission. This loss of

transmission has been partly compensated for by using small band pass filters for filters 1 and 2 and a more than 4 times wider broad band filter for the filters 3 and 4. However, according to eq 1, the real dynamic range for the pixel resolution is mainly determined by a maximum S/N ratio. At this time, an alternative (near-)IR lens material (MgF_2) is in experimental testing. This material has at 2500 nm >90% transmission compared to BK7 (30%). It is expected that with the new optics, the influence of the peak between 2300 and 2500 nm in eq 12 will increase, giving finally better discriminating B values.

CONCLUSIONS

Remote spectroscopic near-infrared imaging spectroscopy, if combined with robust chemometric methods, can serve as a tool for identification of plastics among nonplastics in mixed household waste. The presented mathematical method MIRA helps to extract the spectral fingerprint of a sample from its three-dimensional stack of near-IR images. MIRA provides a rotation of the abstract principal component space into a spectroscopically interpretable solution. MIRA provides identical classifications for differently sized, distinctly shaped, and distinctly located samples made from the same material (plastics detection among nonplastics). Further, MIRA suppresses the negative influences of irregular illumination and shadows in the images. MIRA tolerates a slight sample movement (from conveyor belt) during one measurement. All these properties make the new approach attractive for a real-world implementation in a future real-time, on-line sorting device for mixed postconsumer waste based on remote near-IR imaging spectroscopy.

ACKNOWLEDGMENT

The authors are grateful to the Commission of European Communities for financial support of the SIRIUS project under the grant no. EVWA-CT-92-0001 in the research program Environment. We thank T. Huth-Fehre, R. Feldhoff, T. Kantimm, L. Quick, F. Winter, and K. Cammann (all of ICB, Münster, Germany) and W. Melssen (Nijmegen) for discussions. We are grateful to H. W. Siesler and his students (NIR research group, University of Essen, Germany) for measuring the transmission spectra of our different camera lenses. Further, we thank our undergraduate student Kees de Crom (Nijmegen) for his technical assistance.

Received for review February 2, 1995. Accepted July 5, 1995.[⊗]

AC950117J

[⊗] Abstract published in *Advance ACS Abstracts,* September 1, 1995.